Emergence of homochirality in large molecular systems

Gabin Laurent[a,1,2], David Lacoste[a,1], and Pierre Gaspard[b,1]

[a]Gulliver, UMR CNRS 7083, École Supérieure de Physique et de Chimie Industrielles de la Ville de Paris, Paris Sciences et Lettres Research University, F-75231 Paris, France; and [b]Center for Nonlinear Phenomena and Complex Systems, Université Libre de Bruxelles, B-1050 Brussels, Belgium

Edited by Pablo G. Debenedetti, Princeton University, Princeton, NJ, and approved December 11, 2020 (received for review June 19, 2020)

The selection of a single molecular handedness, or homochirality across all living matter, is a mystery in the origin of life. Frank's seminal model showed in the '50s how chiral symmetry breaking can occur in nonequilibrium chemical networks. However, an important shortcoming in this classic model is that it considers a small number of species, while there is no reason for the prebiotic system, in which homochirality first appeared, to have had such a simple composition. Furthermore, this model does not provide information on what could have been the size of the molecules involved in this homochiral prebiotic system. Here, we show that large molecular systems are likely to undergo a phase transition toward a homochiral state, as a consequence of the fact that they contain a large number of chiral species. Using chemoinformatics tools, we quantify how abundant chiral species are in the chemical universe of all possible molecules of a given length. Then, we propose that Frank's model should be extended to include a large number of species, in order to possess the transition toward homochirality, as confirmed by numerical simulations. Finally, using random matrix theory, we prove that large nonequilibrium reaction networks possess a generic and robust phase transition toward a homochiral state.

homochirality | origin of life | prebiotic chemistry | random matrices | statistical physics

Life on Earth relies on chiral molecules—that is, species not superposable on their mirror images. A given biological molecule forms with its mirror image a pair of enantiomers. Homochirality precisely means the dominance of one member of the pair across the entire biosphere. For instance, in our cells, biochemical reaction networks only involve left-handed (L-chiral) amino acids and right-handed (D-chiral) sugars, but the reason for this absolute specificity escapes us and is one of the most fascinating questions in the origin of life.

The origin of homochirality comes with two questions and related observations: What caused the initial bias of one enantiomer over the other in the presumably racemic environment of the prebiotic world, and how was this bias sustained and maintained as in today's biological world (1)? It is believed that mineral surfaces on Earth (2) or circularly polarized light in interstellar space (3) could explain the first observation, while models based on nonequilibrium reaction networks can explain the second observation (4–15).

However, there is an important shortcoming in the common discussions addressing the issue of homochirality—namely, that they only consider a small number of chiral species, as in Frank's classic model (4) or in its first experimental realization more than 40 years later by Soai et al. (16). There is no reason to expect that the prebiotic world, in which homochirality first emerged, had such a simple and homogeneous chemical composition. Instead, it is more natural to assume that this composition was complex, heterogeneous, and included a large number of chiral and achiral species. We show in this paper that generic nonequilibrium reaction networks possess a phase transition toward a homochiral state as a consequence of the fact that the number of chiral species becomes large.

Cross-Over between Chiral and Achiral Chemical Worlds

With this aim, we first ask how abundant are chiral species in the chemical universe of all possible molecules? It turns out that chirality is rare among molecules with a small number of atoms, but that possible chiral stereoisomers multiply as their number of atoms increases. Accordingly, we should expect a cross-over between the achiral world of small molecules and the chiral world of large molecules involved in chemical-reaction networks. The cross-over should be characterized by some specific number of atoms, where the fractions of achiral and chiral molecules become equal, as schematically depicted in Fig. 1*A*. Beyond the cross-over, the chiral molecules are dominant over achiral ones. The issue of this cross-over is important, in particular, because it associates the emergence of homochirality with some molecular size. Starting with monosubstituted alkanes and alkanes for which an exact enumeration of stereoisomers is available (17, 18), we find that the cross-over measured in number of carbon atoms in these molecules lies between 4.7 and 5.7 for monosubstituted alkanes and between 8.4 and 9.5 for alkanes.

In the chemical universe of Fink and Reymond (19), which contains all virtual molecules of a given number of heavy atoms (i.e., atoms heavier than hydrogen), and satisfying some basic set of rules of chemistry, we find a cross-over at 8.5 heavy atoms. Since a similar study was not available for real molecules, we turn to the chemical database PubChem (20). From the raw data of this large database, we find that a cross-over occurs for molecules of 9.4 heavy atoms (*SI Appendix*, section S1). However, since many chiral molecules do not have all of their enantiomers or stereoisomers, we have also analyzed an expanded database, in which every chiral molecule contains either all its enantiomers or all its stereoisomers. In Fig. 1*B*, the fractions of chiral and

Significance

The selection of a single molecular handedness among the two possible configurations of a given molecule, or homochirality, is observed across all living matter and is a mystery in the origin of life. Here, we show that large chemical systems are likely to undergo a spontaneous symmetry breaking toward a homochiral state as the number of chiral species increases. Through an analysis of a large chemical database, we find that there is no need of very large molecules for chiral species to dominate over achiral ones; it already happens when molecules contain about 10 heavy atoms.

Author contributions: D.L. and P.G. designed research; G.L., D.L., and P.G. performed research; G.L. analyzed data; and G.L., D.L., and P.G. wrote the paper.

The authors declare no competing interest.

This article is a PNAS Direct Submission.

Published under the PNAS license.

[1]G.L., D.L., and P.G. contributed equally to this work.

[2]To whom correspondence may be addressed. Email: gabin.laurent@espci.fr.

This article contains supporting information online at https://www.pnas.org/lookup/suppl/doi:10.1073/pnas.2012741118/-/DCSupplemental.

Published January 11, 2021.

Downloaded at UNIVERSITAT MUENCHEN Bibliothek Bereich Physiologie on February 22, 2021

PHYSICS

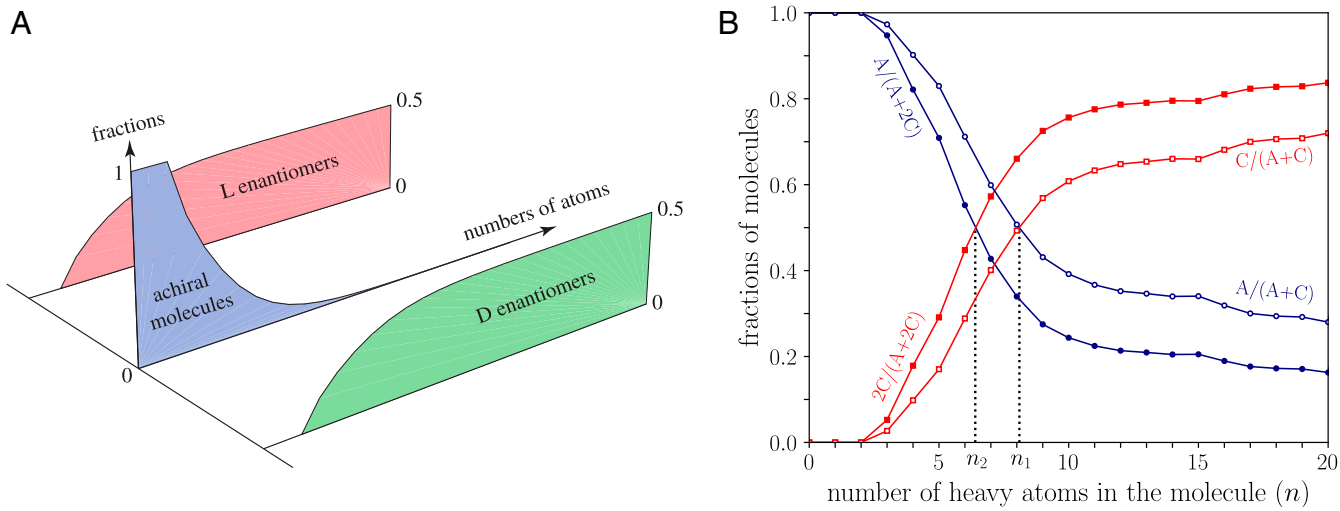

Fig. 1. Cross-over between the achiral and chiral chemical worlds. (*A*) A three-dimensional schematic representation of the fractions of possible achiral and chiral molecules as function of their number of atoms. Every chiral molecule appears as mirror-reflected D- and L-enantiomers. (*B*) A two-dimensional representation of the fractions of achiral (circles) and chiral (squares) molecules in an expanded PubChem database containing all of the stereoisomers of molecules with at most $n \leq 20$ heavy atoms. Filled symbols correspond to counting stereoisomers twice, while open symbols correspond to counting them once in the fractions. Error bars are smaller than symbol sizes, and the cross-over occurs at $n_2 \simeq 6.4$ and $n_1 \simeq 8.1$, depending on which counting is considered (*SI Appendix*, section S1).

achiral species are shown for the case of the database expanded in stereoisomers. Our results for the various estimates for the cross-over are gathered in Table 1 and extracted from Fig. 1*B* and *SI Appendix*, Figs. S1, S2, S3, and S4. Remarkably, irrespective of the precise procedure to generate and analyze the database and regardless of the precise composition of the molecules, the cross-over between the achiral and chiral worlds occurs for a number of heavy atoms of the order of about 10. The main consequence of this cross-over is that the stereoisomer distribution goes from unimodal (with a maximum for achiral molecules) to bimodal (with maxima for opposite enantiomers) as the length of molecules increases. This emerging bimodality is potentially susceptible to induce a chiral symmetry breaking.

Spontaneous Symmetry Breaking into a Chiral State

We now come to our central point—namely, on how to explain the emergence of homochirality from the multiplication of chiral species in nonequilibrium reaction networks. Specifically, we consider a reaction network involving achiral and chiral species described by the concentration vector $\mathbf{c}$, which contains the vector $\mathbf{c}_\mathrm{D}$ (resp. $\mathbf{c}_\mathrm{L}$) for the N_C D-enantiomers (resp. for the N_C L-enantiomers) and the vector $\mathbf{c}_\mathrm{A}$ for the remaining N_A achiral species. In such a system, the evolution of the concentrations is ruled by

$$\frac{d\mathbf{c}}{dt} = \mathbf{F}(\mathbf{c}) + \frac{1}{\tau}(\mathbf{c}_0 - \mathbf{c}), \qquad [1]$$

where $\mathbf{c}_0$ is the concentration vector of the species supplied from the environment at the rate $1/\tau$ and responsible for driving the system out of equilibrium, and $\mathbf{F}(\mathbf{c}) = \boldsymbol{\nu} \cdot \mathbf{w}(\mathbf{c})$ are the reaction rates with specific chiral symmetry (Eq. **14** in *Materials and Methods*), which need not obey mass-action law. In this expression, $\boldsymbol{\nu}$ is the matrix of stoichiometric coefficients and $\mathbf{w}(\mathbf{c})$ the set of net reaction rates. After reaction, the species in excess are flowing out of the system at the same rate $1/\tau$ as for the supply, so that τ represents the mean residence time of the species in the system.

The stability of these equations may be characterized by linearizing them about the racemic state, which is defined by the condition $\mathbf{c}_\mathrm{D} = \mathbf{c}_\mathrm{L}$ and is assumed to exist in a steady state. With the small parameter $\delta\mathbf{x}$, where $\mathbf{x}$ denotes the chiral enantiomeric excess $\mathbf{x} \equiv \frac{1}{2}(\mathbf{c}_\mathrm{L} - \mathbf{c}_\mathrm{D})$, we obtain

$$\frac{d}{dt}\delta\mathbf{x} = \left(\mathbf{J} - \frac{1}{\tau}\right) \cdot \delta\mathbf{x} + \frac{1}{\tau}\,\delta\mathbf{x}_0, \qquad [2]$$

where $\mathbf{J}$ represents the Jacobian matrix deduced from the kinetic Eq. **1**. The racemic mixture is unstable if at least one of the eigenvalues of the matrix $\mathbf{M} = \mathbf{J} - \frac{1}{\tau}\mathbf{I}$ (with $\mathbf{I}$ the identity matrix) has a positive real part. In a large reaction network, the reaction rates may take very different values, so that the matrix $\mathbf{J}$ may be treated as a random matrix (21–23). The simplest model is to assume that the elements of this matrix are independent and identically distributed real numbers (but not necessarily Gaussian distributed) of mean value μ and variance σ^2 (24). When $\mu = 0$, random matrix theory shows that the complex eigenvalues are uniformly distributed in a disk of radius $\sigma\sqrt{N_\mathrm{C}}$ in the limit of large values of N_C (25). When $\mu \neq 0$, we find that there exists a single and isolated eigenvalue, which is equal to μN_C, and the corresponding eigenvector has uniform components to dominant order (*SI Appendix*, section S2). Two possible mechanisms for the instability of the racemic state then emerge for large N_C (*SI Appendix*, section S3). Either mechanism (*i*), the instability occurs due to the isolated eigenvalue, as illustrated in Fig. 2 *D–F*; otherwise, mechanism (*ii*) occurs due to the eigenvalues located on the edge of the circle (which may be real or complex valued),

Table 1. Positions of the cross-over n_1 and n_2, measured in terms of number of carbon atoms, in the study of alkanes and monosubstituted alkanes, or in terms of number of heavy atoms in the other studies.

Data	n_1	n_2
Monosubstituted alkanes stereoisomers	5.7	4.7
Alkanes stereoisomers	9.5	8.4
Chemical universe	8.5	—
PubChem database using raw data	9.4*	—
PubChem database using generated enantiomers	12.7	6.7
PubChem database using generated stereoisomers	8.1	6.4

The estimate n_1 (resp. n_2) is obtained by counting one (resp. twice) the pairs of enantiomers.

*The cross-over for PubChem raw data occurs between n_1 and n_2 because not all enantiomers of a given species are present in the database.

Downloaded at UNIVERSITAT MUENCHEN Bibliothek Bereich Physiologie on February 22, 2021

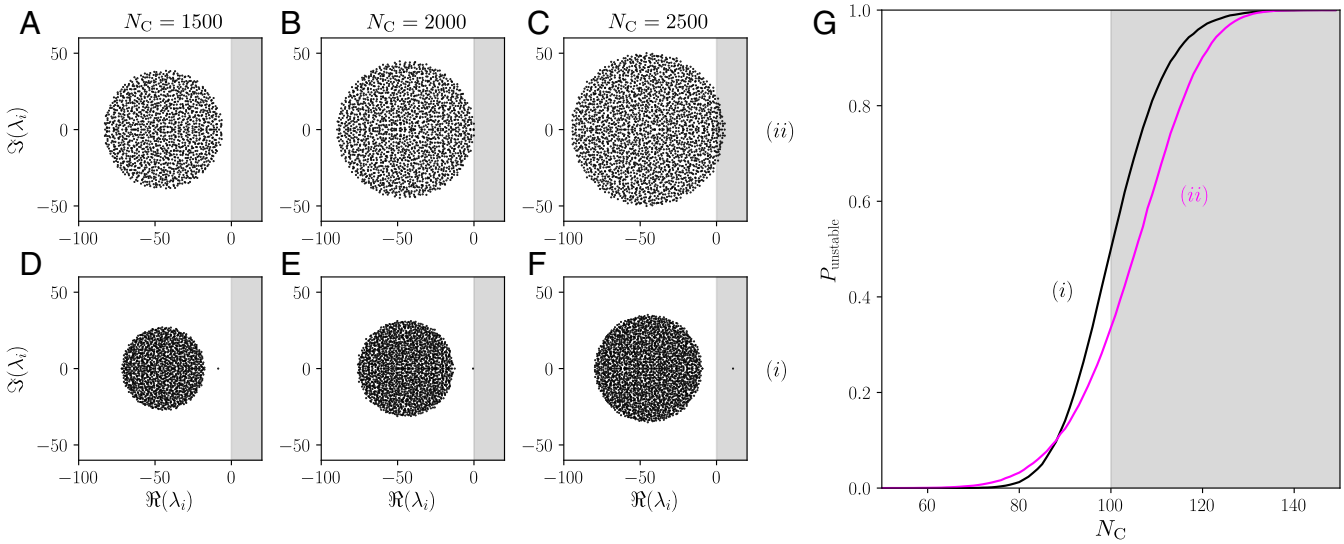

Fig. 2. Distribution of eigenvalues and corresponding instability criterion. *A–C* represent the eigenvalues of the random matrix **M** with Gaussian entries with $\mu = 0$, $\sigma = 1$, and $\tau = 1/\sqrt{2{,}000}$, where the instability mechanism (*ii*) occurs as N_C increases, i.e., the edge of the Girko's circle densely filled by eigenvalues crosses the zero real axis. *D–F* depict the mechanism (*i*), where the zero real axis is crossed by an isolated eigenvalue. In this case, the matrix **M** is a random matrix with Gaussian entries of parameters $\mu = 1/\sqrt{2{,}000}$, $\sigma = 0.7$, and $\tau = 1/\sqrt{2{,}000}$. The gray-colored area represents the positive real part zone of the complex plane, i.e., the area in which an eigenvalue causes the instability. Sizes of random matrices **M** are N_C = 1,500 for *A* and *D*, N_C = 2,000 for *B* and *E*, and N_C = 2,500 for *C* and *F*. *G* represents the probability for the racemic state of the chemical system to be unstable as a function of N_C. The black curve represents the mechanism (*i*) for a Gaussian random matrix **M** with $\mu = 1/\sqrt{100}$, $\sigma = 0.7$, and $\tau = 1/\sqrt{100}$. The magenta curve represents the mechanism (*ii*) for a Gaussian random matrix **M** with $\mu = 0$, $\sigma = 1$ and $\tau = 1/\sqrt{100}$. The gray-colored area represents the theoretical instability area, which is $N > 100$ for both mechanisms here, given the choice of parameters μ, σ, and τ. The statistics has been carried out over 100, 000 realizations of random matrices. Note also that the two curves in *G* for the two mechanisms were drawn for different parameters, μ and σ.

as illustrated in Fig. 2 *A–C*. It follows from this that when $\mu > 0$ and $N_C \geq \max\{1/(\tau\mu), (\sigma/\mu)^2\}$, the system becomes unstable by the first mechanism, where all species become simultaneously unstable, and when $(\sigma/\mu)^2 \geq N_C \geq 1/(\tau\sigma)^2$, the system becomes unstable by the second mechanism, and, in this case, only a subpart of all of the species become unstable at the transition. In such cases, random matrix theory predicts that as N_C becomes large, these mechanisms of instability become more and more likely. This is confirmed by the shape of the probability for the racemic state to be unstable versus N_C shown in Fig. 2*G* for both mechanisms. If the matrix elements are statistically correlated, the nondominant eigenvalues may have a different distribution, but the isolated eigenvalue behaves similarly.

The Effect of Chiral Species Multiplication

In order to show that this general scenario can be realized in practice in a nonequilibrium reaction network, we now introduce generalizations of Frank's model, in which we have multiplied the number of chiral and achiral species, and we have assumed an arbitrary assignation L or D to each enantiomer. We also include reverse reactions in order to guarantee the compatibility with the existence of an equilibrium state, even though the system is driven out of equilibrium. It is essential that the system be driven out of equilibrium in order for chirality to be maintained. We, thus, assume that the system is thermodynamically open, due to fluxes of matter in and out of the system.

Let us also suppose that species entering the autocatalytic system are achiral, but of high free energy, while the achiral species produced by the reactions involving the two D- and L-enantiomers have a lower free energy. In this regard, the achiral species $\{A_a\}_{a=1}^{N_A}$ are of high free energy, and the achiral species $\{\tilde{A}_a\}_{a=1}^{\tilde{N}_{\tilde{A}}}$ of low free energy. The reaction networks are given by the following reactions:

$$\mathrm{A}_a + \mathrm{E}_i \rightleftharpoons \mathrm{E}_j + \mathrm{E}_k, \qquad \textbf{[3]}$$

$$\mathrm{A}_a + \bar{\mathrm{E}}_i \rightleftharpoons \bar{\mathrm{E}}_j + \bar{\mathrm{E}}_k, \qquad \textbf{[4]}$$

$$\mathrm{E}_i + \bar{\mathrm{E}}_j \rightleftharpoons \tilde{\mathrm{A}}_b + \tilde{\mathrm{A}}_c, \qquad \textbf{[5]}$$

where the enantiomer species are either $\mathrm{E}_m = \mathrm{D}_m$ and $\bar{\mathrm{E}}_m = \mathrm{L}_m$, or $\mathrm{E}_m = \mathrm{L}_m$ and $\bar{\mathrm{E}}_m = \mathrm{D}_m$ for each enantiomeric pair $m = i, j, k = 1, 2, \ldots, N_C$; $a = 1, 2, \ldots, N_A$; and $b, c = 1, 2, \ldots, \tilde{N}_{\tilde{A}}$. Eqs. **3–5** define a total of $2^{N_C - 1}$ inequivalent reaction networks differing by the permutations of D- and L-enantiomers for some enantiomeric pairs. For given reaction rates, all of these networks manifest similar dynamical behaviors. Among them, the network with $\mathrm{E}_m = \mathrm{D}_m$ and $\bar{\mathrm{E}}_m = \mathrm{L}_m$ for all of the pairs $m = 1, 2, \ldots, N_C$ is the direct generalization of Frank's model, considered below.

For our numerical implementation of this model, we focus on the fully irreversible regime, in which reactions **[3]**, **[4]**, and **[5]** only proceed forward due to the supply of achiral species with high free energy at the same concentration A_0. Thus, there are two main control parameters in this model: the supply concentration A_0 and the residence time τ.

For one particular realization of these rate constants, Fig. 3*A* shows the evolution of the concentrations of the species present in the system as function of time above the threshold concentration A_0, while Fig. 3*B* shows the case below threshold. In Fig. 3*A*, we see that on long times, the system converges toward a steady state, which is homogeneous and chiral. Only two species have been shown in these figures for clarity, but the time evolution of their concentrations is typical of the evolution of all of the other species: On long times, only one enantiomer is present, which is of the same chirality for all of the species, while the other enantiomer reaches a vanishing concentration. Instead, in Fig. 3*B*, all of the species converge on long times toward a vanishing concentration.

The case where all of the rate constants would be identical can be treated analytically, as done in *SI Appendix*, section S5, so let us now instead assume that the rate constants k_+ of reactions

PHYSICS

Downloaded at UNIVERSITAT MUENCHEN Bibliothek Bereich Physiologie on February 22, 2021

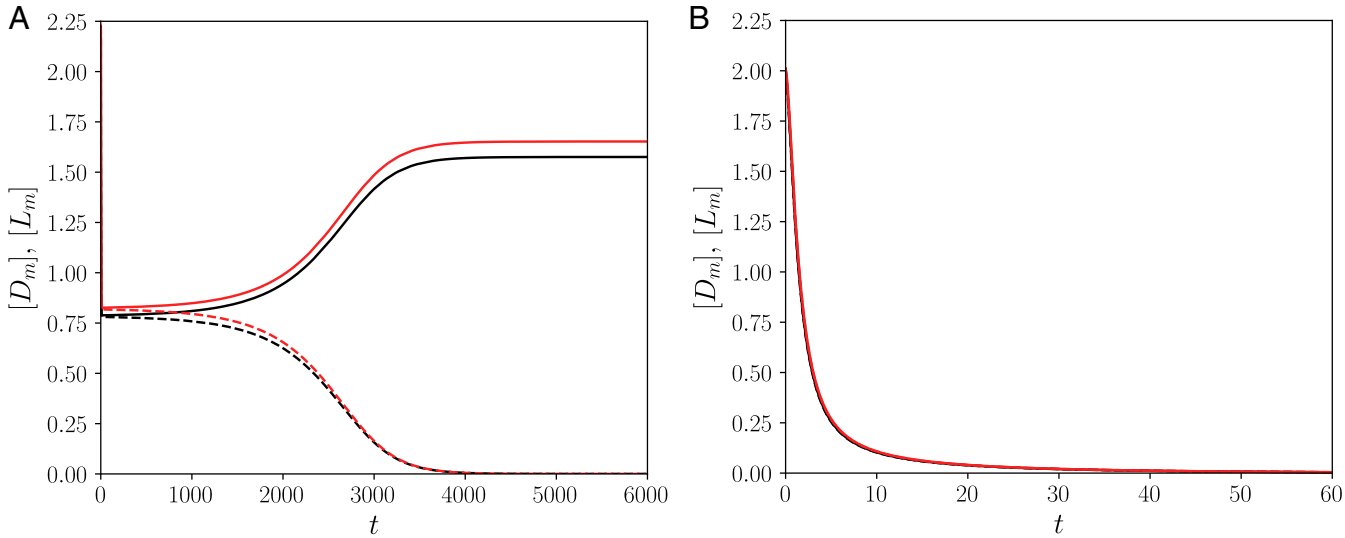

Fig. 3. Dynamical simulations of the autocatalytic network [**22**]-[**22**]-[**23**]. Typical time evolution of two species contained in the autocatalytic network as a function of time above the threshold concentration A_0 (*A*) and below it (*B*) is shown. The solid lines represent one of the two enantiomers for a given species and the dashed line the other enantiomer. Both simulations were carried out with an initial enantiomeric excess $\epsilon = 10^{-2}$, and concentrations of all chiral species were initialized at $D_0 = 2 + \epsilon$ and $L_0 = 2 - \epsilon$. The unactivated achiral species was initialized at $\tilde{A}_0 = 0$ and the activated one at $A_0 = 80$ in *A* and $A_0 = 45$ in *B*. All of the constants k_{+ijk} and $\tilde{k}_{-ij}$ follow a log-normal distribution of parameters $\mu = -10.02$ and $\sigma = 1.27$ (i.e., corresponding to a log-normal distribution with $\langle k_+ \rangle = \langle \tilde{k}_- \rangle = 10^{-4}$ and $\sigma_{k_+} = \sigma_{\tilde{k}_-} = 2 \times 10^{-4}$), with $\tilde{k}_{ij} = \tilde{k}_{ji}$ to satisfy the mirror symmetry described in *SI Appendix*, Eq. **S16**. The number of chiral species was set up to $N_C = 20$.

[**3**] and [**4**] are taken according to a log-normal distribution (26). We find that the spontaneous chiral symmetry breaking happens if the following criterion is satisfied,

$$\langle k_+ \rangle \, \tau \, N_A \, A_0 > \frac{2}{N_C(N_C+1)}, \qquad \textbf{[6]}$$

i.e., the residence time multiplied by the total concentration $N_A \, A_0$ of achiral species supplied to the system must exceed a threshold determined by the average rate constant $\langle k_+ \rangle$ of autocatalysis and the number N_C of chiral species in the reaction network. We have tested this result by performing a linear stability analysis of the racemic steady state. Simulations show that instability is due to an isolated top eigenvalue and confirm the criterion [**6**] when the distribution of the rate constants is not too broad, as shown in Fig. 4, *Inset*. For a very broad distribution, the threshold is pushed toward higher value than predicted by Eq. **6**, but the transition still occurs at sufficiently large N_C (*SI Appendix*, Fig. S5). Importantly, the transition becomes sharp as the number of chiral species increases, as shown in Fig. 4. Thus, the random matrix theory argument holds, and mechanism (*i*) is confirmed, although the eigenvalues of the Jacobian matrix do not cover uniformly a circle (*SI Appendix*, Fig. S6) due to the difference of statistics between the diagonal and the off-diagonal elements (*SI Appendix*, section S5). In this case, mechanism (*ii*) is found not to be relevant. Furthermore, the multiplication of chiral species is also multiplying the number of reaction networks manifesting similar chiral symmetry breaking, but with either the D- or the L-enantiomer for the different chiral species.

Discussion

Let us now come back to our evaluation of the cross-over to chirality in the context of the origin of life. First of all, we observe that among the 20 natural amino acids, the only one that is achiral—i.e., glycine—is also the smallest, containing only five heavy atoms. Secondly, the first chiral molecule observed in space is propylene oxide, containing four heavy atoms (27). Thirdly, among the 11 carboxylic acids of the Krebs cycle, the majority of them, 9, lie in the range between 8 and 13 heavy atoms; only 2 of them are smaller, acetate and pyruvate. In fact, the Krebs cycle appears to function precisely at the border between the world of achiral and small molecules and that

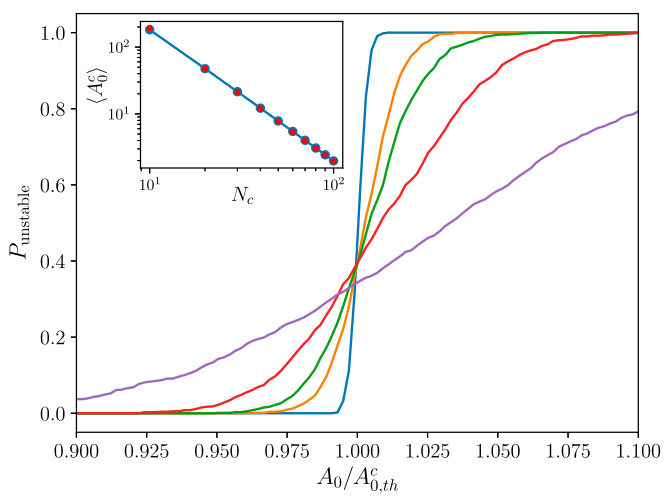

Fig. 4. Probability of instability of the racemic state for the generalized Frank model [**22**]-[**22**]-[**23**]. Probability of the initial racemic state to be unstable by mechanism (*i*) as a function of the normalized value of the control parameter A_0 for the expanded Frank's model in the irreversible regime and for different values of number of chiral species N_C: $N_C = 10$ (magenta), $N_C = 20$ (red), $N_C = 30$ (green), $N_C = 40$ (yellow), and $N_C = 100$ (blue). The control parameter A_0 has been normalized by the theoretical threshold at the transition, defined by the equality in the inequality of Eq. **6**. An average over 1,000 realizations of the rate constants following a log-normal distribution such that $\langle k_+ \rangle = \langle \tilde{k}_- \rangle = 10^{-4}$ and $\sigma_{k_+} = \sigma_{\tilde{k}_-} = 2 \times 10^{-4}$ has been performed. (*Inset*) Comparison between the observed control parameter value A_0 at the transition (red circles) with the theoretical prediction given by Eq. **6** (blue solid line) after averaging over 100 realizations of the rate constants.

Downloaded at UNIVERSITAT MUENCHEN Bibliothek Bereich Physiologie on February 22, 2021

of large and chiral molecules (28). The emergence of the Krebs cycle, thus, represents a major step, which facilitates the synthesis of a large number of long chiral molecules (29).

We presented a scenario that explains why a large complex molecular system tends to become chiral. Based on fundamental properties of phase transitions, confirmed by numerical simulations of a nonequilibrium reaction network, our scenario is both general and robust. Details of the reaction network should not matter, nor the precise way in which the system is driven out of equilibrium, provided the system is large enough. In addition, the homochiral state of our model does not need to be all D or L across all species, in agreement with the observation that, for instance, amino acids are L-chiral, but sugars are D-chiral. Moreover, our reaction scheme need not satisfy mass-action law, and there is also no requirement that the system be fully well-mixed; it could be compartmentalized. As an illustration of this idea, we study two diffusively coupled chemical reactors, identical to the one considered so far (*SI Appendix*, section S6). For low coupling, the two compartments undergo separately the homochiral transition, while at high coupling, they reach the same homochiral state (13). Compartmentalized systems enrich the scenarios for the transition to homochirality, because, on the one hand, as shown recently, compartmentalization significantly broadens the diversity of available autocatalytic networks, which can be built with a limited number of compounds (30), and, on the other hand, in such systems, the number of species is effectively increased, which favors our mechanism.

Our scenario thus offers a universal pathway toward homochirality potentially unifying many previous approaches on this issue. In the context of the origin of life, we also find that there is no need for very long and complex molecules for this homochiral state to emerge. The transition can already occur in a prebiotic world containing molecules with about 10 heavy atoms.

Materials and Methods

Chemoinformatics of Chirality. A study of the scaling of the number of chiral and achiral species with the number of atoms for monosubstituted alkanes and alkanes stereoisomers is provided in *SI Appendix*, section S1, together with details on the chemoinformatic analysis of the PubChem database (20).

Chiral Symmetry Breaking for a General Reaction Scheme. The spontaneous symmetry breaking of chirality can be described in the framework of kinetics. The reaction network is supposed to involve achiral and chiral species at the concentrations

$$\mathbf{c} = \begin{pmatrix} \mathbf{c}_{\mathrm{D}} \\ \mathbf{c}_{\mathrm{A}} \\ \mathbf{c}_{\mathrm{L}} \end{pmatrix}, \qquad [7]$$

which, respectively, denote the concentrations of D-enantiomers, achiral species, and L-enantiomers. If N_{D}, N_{A}, and N_{L} denote the respective numbers of these species, the system is described in terms of $N_{\mathrm{S}} = N_{\mathrm{D}} + N_{\mathrm{A}} + N_{\mathrm{L}} = N_{\mathrm{A}} + 2N_{\mathrm{C}}$ concentrations with $N_{\mathrm{C}} \equiv N_{\mathrm{D}} = N_{\mathrm{L}}$.

In an open system, the time evolution of these concentrations is ruled by the N_{S} kinetic equations in Eq. **1** with $\mathbf{F}(\mathbf{c}) = \boldsymbol{\nu} \cdot \mathbf{w}(\mathbf{c})$, expressed in terms of the matrix $\boldsymbol{\nu}$ of stoichiometric coefficients, the set $\mathbf{w}(\mathbf{c})$ of net reaction rates $w_r(\mathbf{c}) = w_{+r}(\mathbf{c}) - w_{-r}(\mathbf{c})$ with $r = 1, 2, \ldots, N_{\mathrm{R}}$, the supply concentrations $\mathbf{c}_0$, and the residence time τ of the species in the system. The system is closed if the residence time is infinite, in which case the last term drops in Eq. **1**.

The mirror symmetry of the system corresponds to the following exchange of concentrations of D- and L-enantiomers,

$$\mathbf{S}_{\mathbf{c}} \cdot \mathbf{c} = \begin{pmatrix} 0 & 0 & \mathbf{I} \\ 0 & \mathbf{I} & 0 \\ \mathbf{I} & 0 & 0 \end{pmatrix} \cdot \begin{pmatrix} \mathbf{c}_{\mathrm{D}} \\ \mathbf{c}_{\mathrm{A}} \\ \mathbf{c}_{\mathrm{L}} \end{pmatrix} = \begin{pmatrix} \mathbf{c}_{\mathrm{L}} \\ \mathbf{c}_{\mathrm{A}} \\ \mathbf{c}_{\mathrm{D}} \end{pmatrix}, \qquad [8]$$

written in terms of the $N_{\mathrm{S}} \times N_{\mathrm{S}}$ matrix, such that $\mathbf{S}_{\mathbf{c}}^2 = \mathbf{I}$, where $\mathbf{I}$ denotes the corresponding identity matrix. Since the rate constants take equal values for mirror-symmetric reactions, the reaction rates have the symmetry

$$\mathbf{w}(\mathbf{S}_{\mathbf{c}} \cdot \mathbf{c}) = \mathbf{S}_{\mathbf{w}} \cdot \mathbf{w}(\mathbf{c}), \qquad [9]$$

with some $N_{\mathrm{R}} \times N_{\mathrm{R}}$ matrix satisfying $\mathbf{S}_{\mathbf{w}}^2 = \mathbf{I}$. As a consequence of the mirror symmetry, the $N_{\mathrm{S}} \times N_{\mathrm{R}}$ matrix of stoichiometric coefficients obeys the following symmetry relation

$$\mathbf{S}_{\mathbf{c}} \cdot \boldsymbol{\nu} \cdot \mathbf{S}_{\mathbf{w}} = \boldsymbol{\nu}. \qquad [10]$$

We note that the kinetic equations may also be written in the following form,

$$\frac{d\mathbf{c}_{\mathrm{D}}}{dt} = \mathbf{F}_{\mathrm{D}}(\mathbf{c}_{\mathrm{D}}, \mathbf{c}_{\mathrm{A}}, \mathbf{c}_{\mathrm{L}}) + \frac{1}{\tau}(\mathbf{c}_{\mathrm{D0}} - \mathbf{c}_{\mathrm{D}}), \qquad [11]$$

$$\frac{d\mathbf{c}_{\mathrm{A}}}{dt} = \mathbf{F}_{\mathrm{A}}(\mathbf{c}_{\mathrm{D}}, \mathbf{c}_{\mathrm{A}}, \mathbf{c}_{\mathrm{L}}) + \frac{1}{\tau}(\mathbf{c}_{\mathrm{A0}} - \mathbf{c}_{\mathrm{A}}), \qquad [12]$$

$$\frac{d\mathbf{c}_{\mathrm{L}}}{dt} = \mathbf{F}_{\mathrm{L}}(\mathbf{c}_{\mathrm{D}}, \mathbf{c}_{\mathrm{A}}, \mathbf{c}_{\mathrm{L}}) + \frac{1}{\tau}(\mathbf{c}_{\mathrm{L0}} - \mathbf{c}_{\mathrm{L}}), \qquad [13]$$

where the mirror symmetry is expressed as

$$\mathbf{F}_{\mathrm{D}}(\mathbf{x}, \mathbf{y}, \mathbf{z}) = \mathbf{F}_{\mathrm{L}}(\mathbf{z}, \mathbf{y}, \mathbf{x}) \quad \text{and} \quad \mathbf{F}_{\mathrm{A}}(\mathbf{x}, \mathbf{y}, \mathbf{z}) = \mathbf{F}_{\mathrm{A}}(\mathbf{z}, \mathbf{y}, \mathbf{x}). \qquad [14]$$

The symmetry can be explicitly broken by input concentrations, such that $\mathbf{S}_{\mathbf{c}} \cdot \mathbf{c}_0 \neq \mathbf{c}_0$. However, the equations remain symmetric if the condition $\mathbf{S}_{\mathbf{c}} \cdot \mathbf{c}_0 = \mathbf{c}_0$ holds. In this case, the racemic mixture characterized by equal concentrations of D- and L-enantiomers,

$$\mathbf{c}_{\mathrm{D}} = \mathbf{c}_{\mathrm{L}}, \qquad [15]$$

is maintained during the time evolution of the reaction network, if the dynamics

$$\frac{d\mathbf{c}_{\mathrm{A}}}{dt} = \mathbf{F}_{\mathrm{A}}(\mathbf{c}_{\mathrm{D}}, \mathbf{c}_{\mathrm{A}}, \mathbf{c}_{\mathrm{D}}) + \frac{1}{\tau}(\mathbf{c}_{\mathrm{A0}} - \mathbf{c}_{\mathrm{A}}), \qquad [16]$$

$$\frac{d\mathbf{c}_{\mathrm{D}}}{dt} = \mathbf{F}_{\mathrm{D}}(\mathbf{c}_{\mathrm{D}}, \mathbf{c}_{\mathrm{A}}, \mathbf{c}_{\mathrm{D}}) + \frac{1}{\tau}(\mathbf{c}_{\mathrm{D0}} - \mathbf{c}_{\mathrm{D}}), \qquad [17]$$

is stable in the racemic subspace [**15**]. In order to investigate this issue, we introduce the variables

$$\mathbf{x} \equiv \frac{1}{2}(\mathbf{c}_{\mathrm{L}} - \mathbf{c}_{\mathrm{D}}), \qquad [18]$$

characterizing deviations with respect to the racemic subspace, and we perform the linear stability analysis for infinitesimal deviations $\delta\mathbf{x}$ with respect to the racemic subspace. These deviations are ruled by the following set of linear equations:

$$\frac{d}{dt}\delta\mathbf{x} = \left(\mathbf{J}_{\mathrm{DD}} - \mathbf{J}_{\mathrm{DL}} - \frac{1}{\tau}\right) \cdot \delta\mathbf{x} + \frac{1}{\tau}\,\delta\mathbf{x}_0, \qquad [19]$$

where

$$\mathbf{J}_{\mathrm{DD}} \equiv \frac{\partial \mathbf{F}_{\mathrm{D}}}{\partial \mathbf{c}_{\mathrm{D}}} = \frac{\partial \mathbf{F}_{\mathrm{L}}}{\partial \mathbf{c}_{\mathrm{L}}} \quad \text{and} \quad \mathbf{J}_{\mathrm{DL}} \equiv \frac{\partial \mathbf{F}_{\mathrm{D}}}{\partial \mathbf{c}_{\mathrm{L}}} = \frac{\partial \mathbf{F}_{\mathrm{L}}}{\partial \mathbf{c}_{\mathrm{D}}}. \qquad [20]$$

Note that the chiral symmetry conditions, namely, Eq. **14**, have been used to derive these equations. We suppose that $\delta\mathbf{x}_0 = 0$, so that there is no explicit symmetry breaking. Moreover, the dynamics in the racemic subspace is assumed to have a steady state. We use the notations $\mathbf{J} = \mathbf{J}_{\mathrm{DD}} - \mathbf{J}_{\mathrm{DL}}$ and $\mathbf{M} \equiv \mathbf{J} - \mathbf{I}/\tau$. The $N_{\mathrm{C}} \times N_{\mathrm{C}}$ $\mathbf{M}$ matrix controls the linear stability of the racemic steady state. It is asymptotically stable if all of the eigenvalues $\{\lambda_i\}$ of that matrix have a negative real part: $\Re\,\lambda_i < 0$ for all $i = 1, 2, \ldots, N_{\mathrm{C}}$. The racemic mixture is unstable if at least one of its eigenvalues has a positive real part.

Generalized Frank's Model. For numerical investigations, we consider the model [**3**]-[**4**]-[**5**] with $\mathrm{E}_i = \mathrm{D}_i$ and $\bar{\mathrm{E}}_i = \mathrm{L}_i$ for all $i = 1, 2, \ldots, N_{\mathrm{C}}$ in the irreversible regime with $N_{\mathrm{A}} = \tilde{N}_{\tilde{\mathrm{A}}} = 1$ and $N \equiv N_{\mathrm{C}} \gg 1$. Moreover, we suppose that the initial concentrations $D_{m0} = L_{m0} = \tilde{A}_0 = 0$ for all species m. Since $D_{m0} = L_{m0}$, there is no explicit chiral symmetry breaking caused by nonracemic inflow from the environment. In this regime, the reaction network reads

$$\mathrm{A} + \mathrm{D}_i \to \mathrm{D}_j + \mathrm{D}_k, \qquad [21]$$

$$\mathrm{A} + \mathrm{L}_i \to \mathrm{L}_j + \mathrm{L}_k, \qquad [22]$$

$$\mathrm{D}_i + \mathrm{L}_j \to 2\,\tilde{\mathrm{A}}, \qquad [23]$$

where $i, j, k = 1, 2, \ldots, N_{\mathrm{C}}$.

Now, the net reaction rates are given by

$$w_{ijk}^{(\mathrm{D})} = k_{+ijk}\, A\, D_i \quad \text{with} \quad j \leq k, \qquad [24]$$

$$w_{ijk}^{(\mathrm{L})} = k_{+ijk}\, A\, L_i \quad \text{with} \quad j \leq k, \qquad [25]$$

$$\tilde{w}_{ij} = \tilde{k}_{-ij}\, D_i\, L_j, \qquad [26]$$

PHYSICS

Downloaded at UNIVERSITÄT MUENCHEN Bibliothek Bereich Physiologie on February 22, 2021

where $\tilde{k}_{-ij} = \tilde{k}_{-ji}$ because of the mirror symmetry. Rate constants are randomly distributed according to a log-normal distribution, as explained in *SI Appendix*, section S4.

The kinetic equations thus have the following form,

$$\dot{A} = -\sum_{\substack{ijk \\ j\leq k}} w_{ijk}^{(\mathrm{D})} - \sum_{\substack{ijk \\ j\leq k}} w_{ijk}^{(\mathrm{L})} + \frac{1}{\tau}(A_0 - A), \quad [27]$$

$$\dot{D}_m = \sum_{\substack{ijk \\ j\leq k}} \nu_{m,ijk}\, w_{ijk}^{(\mathrm{D})} - \sum_i \tilde{w}_{mi} - \frac{1}{\tau} D_m, \quad [28]$$

$$\dot{L}_m = \sum_{\substack{ijk \\ j\leq k}} \nu_{m,ijk}\, w_{ijk}^{(\mathrm{L})} - \sum_i \tilde{w}_{im} - \frac{1}{\tau} L_m, \quad [29]$$

$$\dot{\tilde{A}} = 2\sum_{ij} \tilde{w}_{ij} - \frac{1}{\tau}\tilde{A}, \quad [30]$$

with $\nu_{m,ijk} \equiv -\delta_{mi} + \delta_{mj} + \delta_{mk}$.

Numerical Simulations of the Reaction Network. The above equations for the fully irreversible model have been simulated using a Runge–Kutta algorithm of second order. The numerical integration of the kinetic equations has been performed by setting $\tau = 1$, meaning that we take τ as the time unit. At the initial time, we assume that there is a very small imbalance between the two enantiomers of given species, characterized by the small parameter ϵ, which is homogeneous among all of the species.

The integration of the ordinary differential equations allows us to determine the threshold of instability, as well as every asymptotically stable solution—in particular, the racemic solution with $D_i = L_i$ below the threshold of instability. This threshold can be determined by increasing the control parameter A_0 until the solution of the equations is no longer racemic, giving the critical value of the threshold A_{0c} for the transition-breaking chiral symmetry inside the system.

With this dynamics, we observe that the system never converges toward a nontrivial racemic state, where the concentrations of the two enantiomers of a given species would be nonzero and equal to each other. Thus, starting with a state with a small enantiomeric excess, we either reach the trivial racemic state or a homochiral state. For this reason, Fig. 4 has been made by studying the stability of the trivial racemic state using many random realizations of the rate constants k_{+ijk} following a log-normal distribution, which is more efficient numerically than a time integration of the equations of motion.

Further Materials. In *SI Appendix*, section S2, we study the properties of the Jacobian matrix and deduce from them in *SI Appendix*, section S3 a general instability criterion of the racemic state based on random matrix theory. In *SI Appendix*, section S4, we present the reversible generalized Frank model, and we analyze its properties for uniform rate constants. In *SI Appendix*, section S5, we derive the instability criterion for the generalized Frank model with random rate constants. In *SI Appendix*, section S6, we study two diffusively coupled compartments.

Data Availability. Codes have been deposited in GitHub (https://github.com/gablaurent/homochirality).

ACKNOWLEDGMENTS. We thank A. Blokhuis and A. Duprat for fruitful discussions; and L. Leibler and Y. Geerts for their helpful comments. P.G. was supported by Université Libre de Bruxelles and the Fonds de la Recherche Scientifique under Grant PDR T.0094.16 for the project "SYMSTATPHYS." D.L. was supported by Agence Nationale de la Recherche Grants ANR-10-IDEX-0001-02, Origins and Conditions for the Emergence of Life (IRIS OCAV project), ANR-11-LABX-0038, and ANR-10-IDEX-0001-02.

1. D. G. Blackmond, The origin of biological homochirality. *Cold Spring Harb. Perspect. Biol.* **2**, a002147–a002147 (2010).
2. K. H. Ernst, Molecular chirality in surface science. *Surf. Sci.* **613**, 1–5 (2013).
3. C. Meinert *et al.*, Photochirogenesis: Photochemical models on the absolute asymmetric formation of amino acids in interstellar space. *Phys. Life Rev.* **8**, 307–330 (2011).
4. F. C. Frank, On spontaneous asymmetric synthesis. *Biochim. Biophys. Acta* **11**, 459–463 (1953).
5. D. K. Kondepudi, G. W. Nelson, Chiral symmetry breaking in nonequilibrium systems. *Phys. Rev. Lett.* **50**, 1023–1026 (1983).
6. R. Plasson, D. K. Kondepudi, H. Bersini, A. Commeyras, K. Asakura, Emergence of homochirality in far-from-equilibrium systems: Mechanisms and role in prebiotic chemistry. *Chirality* **19**, 589–600 (2007).
7. D. K. Kondepudi, K. Asakura, Chiral autocatalysis, spontaneous symmetry breaking, and stochastic behavior. *Acc. Chem. Res.* **34**, 946–954 (2001).
8. J. A. D. Wattis, P. V. Coveney, Symmetry-breaking in chiral polymerization. *Origins Life Evol. Bios* **35**, 243–273 (2005).
9. R. Kafri, O. Markovitch, D. Lancet, Spontaneous chiral symmetry breaking in early molecular networks. *Biol. Direct* **5**, 38 (2010).
10. Y. Saito, H. Hyuga, Homochirality: Symmetry breaking in systems driven far from equilibrium. *Rev. Mod. Phys.* **85**, 603–621 (2013).
11. M. Stich, J. M. Ribó, D. G. Blackmond, D. Hochberg, Necessary conditions for the emergence of homochirality via autocatalytic self-replication. *J. Chem. Phys.* **145**, 074111 (2016).
12. D. Hochberg, R. D. Bourdon Garcia, J. A. Agreda Bastidas, J. M. Ribó, Stoichiometric network analysis of spontaneous mirror symmetry breaking in chemical reactions. *Phys. Chem. Chem. Phys.* **19**, 17618–17636 (2017).
13. F. Jafarpour, T. Biancalani, N. Goldenfeld, Noise-induced symmetry breaking far from equilibrium and the emergence of biological homochirality. *Phys. Rev. E* **95**, 032407 (2017).
14. F. Jafarpour, T. Biancalani, N. Goldenfeld, Noise-induced mechanism for biological homochirality of early life self-replicators. *Phys. Rev. Lett.* **115**, 158101 (2015).
15. R. Plasson, H. Bersini, A. Commeyras, Recycling Frank: Spontaneous emergence of homochirality in noncatalytic systems. *Proc. Natl. Acad. Sci. U.S.A.* **101**, 16733–16738 (2004).
16. K. Soai, T. Shibata, H. Morioka, K. Choji, Asymmetric autocatalysis and amplification of enantiomeric excess of a chiral molecule. *Nature* **378**, 767–768 (1995).
17. S. Fujita, Alkanes as stereoisomers. enumeration by the combination of two dichotomies for three-dimensional trees. *MATCH Commun. Math. Comput. Chem.* **57**, 299 (2007).
18. S. Fujita, Numbers of monosubstituted alkanes as stereoisomers. *J. Comput. Chem. Japan.* **6**, 59–72 (2007).
19. T. Fink, J. L. Reymond, Virtual exploration of the chemical universe up to 11 atoms of C, N, O, F. *J. Chem. Inf. Model.* **47**, 342–353 (2007).
20. National Library of Medicine, PubChem, https://pubchem.ncbi.nlm.nih.Gov/ (National Center for Biotechnology Information, Bethesda MD, 2019).
21. S. Allesina, S. Tang, Stability criteria for complex ecosystems. *Nature* **483**, 205–208 (2012).
22. R. May, Will a large complex system be stable?. *Nature* **238**, 413–414 (1972).
23. M. R. Gardner, W. R. Ashby, Connectance of large dynamic (cybernetic) systems: Critical values for stability. *Nature* **228**, 784–784 (1970).
24. J. Ginibre, Statistical ensembles of complex, quaternion, and real matrices. *J. Math. Phys.* **6**, 440–449 (1965).
25. V. L. Girko, Circular law. *Theory Probab. Appl.* **29**, 694–706 (1985).
26. D. Davidi, L. M. Longo, J. Jabłońska, R. Milo, D. S. Tawfik, A bird's-eye view of enzyme evolution: Chemical, physicochemical, and physiological considerations. *Chem. Rev.* **118**, 8786–8797 (2018).
27. B. A. McGuire *et al.*, Discovery of the interstellar chiral molecule propylene oxide (CH_3CHCH_2O). *Science* **32**, 1449–1452 (2016).
28. E. Smith, H. J. Morowitz, *The Origin and Nature of Life on Earth: The Emergence of the Fourth Geosphere* (Cambridge University Press, New York, NY, 2016).
29. H. J. Morowitz, J. D. Kostelnik, J. Yang, G. D. Cody, The origin of intermediary metabolism. *Proc. Natl. Acad. Sci. U.S.A.* **97**, 7704–7708 (2000).
30. A. Blokhuis, D. Lacoste, P. Nghe, Universal motifs and the diversity of autocatalytic systems. *Proc. Natl. Acad. Sci. U.S.A.* **117**, 25230–25236 (2020).

Downloaded at UNIVERSITAT MUENCHEN Bibliothek Bereich Physiologie on February 22, 2021